BASIC SCIENCE

Nanomedicine: Nanotechnology, Biology, and Medicine
13 (2017) 1531–1542

Original Article

nanomedjournal.com

Gold nanoparticle interactions in human blood: a model evaluation

Niloofar Ajdari, MSc[a,1], Cian Vyas, MSc[b,1], Stephanie L. Bogan, MSc[c], Bashir A. Lwaleed, PhD[d], Brian G. Cousins, PhD[c,*]

[a]*Department of Mechanical Engineering, Imperial College London, U.K.*
[b]*School of Mechanical, Aerospace & Civil Engineering, University of Manchester, U.K.*
[c]*Department of Nanotechnology, University College London, U.K.*
[d]*Division of Surgery & Interventional Science, University College London, U.K.*

Received 19 August 2016; accepted 31 January 2017

Abstract

In this study, we investigated gold nanoparticle (AuNP) interactions in blood using thromboelastography as a rapid screening tool to monitor their influence on blood coagulation. 1.2 nM colloidal AuNPs ranging from 12 to 85 nm have no effect in the blood, however, 5 nM AuNPs demonstrate pro-thrombogenic concentration dependent effects with a reduction in clot formation. Size effects exhibit a non-linear trend with 45 and 85 nm particles resulting in a faster pro-thrombotic response. Clot strength decreased with AuNP size with the greatest reduction with 28 nm particles. We assessed AuNP interactions in the blood focusing on their biological activity. AuNP-RGD possessed pro-coagulant activities, while PEG-thiol, human fibrinogen and clopidogrel prevented blood clot formation and influenced platelet activity, and were more efficient when bound to nanocarriers than unbound ligands. Such tests could fill the knowledge gaps in thrombogenicity of NPs between in vitro test methods and predict in vivo haemocompatibility.

Key words: Gold nanoparticles; Thrombogenicity; Protein corona; Thromboelastography; Haemocompatibility; Blood coagulation

The application of nanotechnology in medicine has received global attention in many important areas ranging from new diagnostics using image enhancing contrast agents to targeted delivery and photodynamic therapy.[1–3] Gold nanoparticles (AuNPs) are an important class of material as their unique physicochemical properties such as the adsorption of near infrared light releasing thermal energy offers new opportunities in the treatment of disease.[4] Much research has focused on the versatility of AuNP chemistry (e.g. wettability, energy, charge), reactivity, size, shape, and concentration on protein adsorption and cell behavior.[5,6] Exposure of AuNPs to serum or plasma leads to the formation of soft (sec-min) and hard (h-days) protein corona to create a conditioned interface at which the cells respond.[7–10] Studies have shown that strong links exist between nanoparticle (NP)-protein interactions, immunogenicity and cytotoxicity.[11–13] While other nanomaterials have been found to induce platelet aggregation, alter blood coagulation pathways and produce unwanted side effects.[14–16] Recent strategies tailored toward surface modification use passivating ligands such as polyethylene glycol (PEG), peptides, antibodies and therapeutics to enhance their bioactivity for targeted delivery to direct cell uptake, improve clearance and minimize accumulation in the tissues.[17] However, there is a real shortage of laboratory based tests to evaluate NP interactions in the blood, and their influence on blood coagulation, which is integral to their design, overall safety, and efficiency en route to the clinic.

AuNP interactions have been studied with components of the blood, and focus on platelets, coagulation factors and plasma proteins.[18] AuNPs (30 and 50 nm) incubated in blood plasma, double

The authors are very grateful to the Royal Free Hospital Thrombosis Unit for platelet aggregometry, and the Royal Free Electron Microscopy Unit for TEM.

Conflict of interest and sources of support: The authors declare no conflicts of interest and/or competing financial interests. The authors would like to acknowledge the financial support of the EPSRC CASE Award (EP/L504889/1), and Healthcare Impact Partnership (EP/L024713/1).

*Corresponding author at: University College London, Division of Surgery & Interventional Science, Department of Nanotechnology, Royal Free NHS Trust Hospital, 9th Floor, Rm 304, Pond Street, London, NW3 2PF, United Kingdom.
E-mail address: brian.cousins@ucl.ac.uk (B.G. Cousins).

[1] Both authors contributed equally in the production of this manuscript.

http://dx.doi.org/10.1016/j.nano.2017.01.019

in size, and increase their surface charge, and have no effect on platelet aggregation and coagulation tests.[19] Surface curvature influences the amount of protein, and studies exploring a variety of ligands demonstrate that protein structure, NP composition, size and chemistry have the greatest influence over protein corona.[10,19–24] Fibrinogen, albumin and γ-globulin have strong interactions with AuNPs (5-100 nm) causing changes in protein conformation.[10,19] Modification of AuNPs (30 nm) with PEG indicated that the composition of corona was only slightly influenced by the total amount of bound protein, which did not correlate with blood coagulation tests.[25] Studies with polyphosphate functionalised AuNPs (10-50 nm) show activation of the intrinsic pathway and cause rapid procoagulant effects by reducing clotting times.[26] AuNPs (13 nm) modified with sulphonated chitosan, and pyrimidine (10 nm) show prolonged clotting times, inhibit platelet aggregation, and interfere with thrombin and fibrin to demonstrate anti-thrombogenicity.[27–28] While studies with carboxylated polystyrene NPs show selective activation of the intrinsic pathway through size dependent effects (220 nm) and influence enzyme activity.[29] The limitations in many of these studies are similar to those encountered in the clinic, which rely on plasma coagulation tests. Activated partial thromboplastin time (aPTT) and prothrombin time (PT) are static assays that measure both the intrinsic and extrinsic pathways of the coagulation cascade in isolation, and lack the cellular components (e.g. platelets) and clotting factors present in whole blood.[30] Prolonged aPTT and PT times are insensitive to small changes in coagulation, and do not always predict prothrombogenic states.[30] Platelet aggregation tests may not detect small changes in the level of activation, hence the need for more sensitive test methods to monitor NP interactions in the blood.

Hemostasis is a delicate balance between procoagulant, anti-coagulant and fibrinolytic pathways in response to trauma to prevent blood loss. Blood coagulation is triggered in response to injury to release tissue factor or by activation in response to a foreign material to trigger the extrinsic or intrinsic pathways resulting in a cascade of enzymatic reactions.[16,31–32] Both pathways converge in to the common pathway through enzymatic cleavage of prothrombin in to thrombin to activate the conversion of fibrinogen in to fibrin monomers to form a mesh network and platelet plug resulting in a stable clot.[16,31–32] Surface sensitive and physical techniques are available to study blood coagulation such as quartz crystal microbalance (QCM) to measure changes in mass.[28] Viscoelastic changes in developing blood clots can be monitored under low shear stress conditions using thromboelastography (TEG®) to measure all aspects of coagulation and hemostasis following therapeutic intervention.[33–35] Recent standardization of TEG® has been used to determine the thrombogenicity of vascular biomaterials and nanocomposites, as well as, zinc oxide (70 nm) and silicon dioxide (232 nm) NPs to highlight procoagulant and anti-thrombogenic activity.[36–38]

Currently, there are no studies, which investigate the influence of AuNPs in citrated whole blood (CWB) when all of the cellular and plasma components are present despite being the first nano-bio interface encountered via intravenous routes of delivery.[16] We selected AuNPs as they are already used as nanomedicines for targeted drug delivery, and in the treatment of cancer as Au nanoshells.[39–40] In this study, we investigate the effects of AuNP size (10-100 nm) and composition and their interactions in plasma and CWB using TEG®.[41] Our original hypothesis was that AuNPs would produce size and concentration dependent effects, as well as, a differential response to each other. Finally, we assessed the influence of AuNPs with tailored biological activity, and demonstrate the use of TEG® as a rapid screening tool to monitor NP blood-interactions under constant physiological conditions in vitro.

Methods

Preparation of colloidal Au

All reagents were purchased from Sigma–Aldrich UK, unless otherwise specified. Sterile de-ionized water (dH_2O) was purchased from Baxter Healthcare UK. Five colloidal Au sols (I-V) were prepared using methods described by Turkevich and Frens to produce AuNPs ranging from 16 to 100 nm in diameter by reduction of Au (III) chloride trihydrate ($HAuCl_4.3H_2O$) using sodium citrate ($Na_3C_6H_5O_7$) as the reductant as shown in (Eq. (1))[42,43]:

$$Au^{+3}{}_{(aq)} + \text{citrate ions}\left[C_3H_5OCOO_3{}^{3-}\right]_{(aq)} \rightarrow Au^{0}{}_{(s)} \quad (1)$$

0.10 g $HAuCl_4.3H_2O$ was dissolved in 1 L dH_2O to form a 0.25 mM stock, and 10 g $Na_3C_6H_5O_7$ was prepared in 1 L dH_2O as the reducing agent. AuNP synthesis was conducted in a laminar flow hood by transferring 50 ml of 0.25 mM stock to a 250 ml conical flask, which was heated to 100 °C on a hot plate with continuous gentle stirring. A fixed volume of $Na_3C_6H_5O_7$ was added to the stock solution, which changed color after 25 s from blue to orange followed by red (sample I-III) and blue to violet (IV-V) indicative of particle nucleation and growth (Figure 1, *A-B*).[43] All samples were heated for 5 min after the reaction to allow for complete reduction of $HAuCl_4.3H_2O$, and allowed to cool before being stored at 4 °C.

Characterization of AuNPs

UV–visible spectroscopy

Au sols were characterized through UV–vis spectroscopy (Jasco, UK model no. V-630) to obtain spectra of localized surface plasmon resonance (LSPR) generated by AuNPs (Figure 1, *C*). Quartz crystal cuvettes with a path length of 10 mm were used to obtain adsorption spectra using 2 ml 1% wt. sodium citrate as a baseline measurement. 2 ml Au sol was analyzed using scan speeds of 400 nm/min to record wavelengths over 1100 to 200 nm, and was used as a quality control test to ensure consistency (n = 3).

Transmission electron microscopy (TEM) analysis of AuNPs

Copper grids (Gilder Grids, UK, 300 mesh) were prepared by placing 100 μl of 1.2 nM Au sol on to the surface, and allowing to settle for 2 min before wicking off excess liquid with filter paper. The grids were allowed to air dry before analysis using an FEI/Phillips CM120 TEM using energy-dispersive X-ray (EDX) spectroscopy and image capturing software (Advanced Microscopy Techniques, USA) in random fields of view at ×58,000 magnification (n = 60).

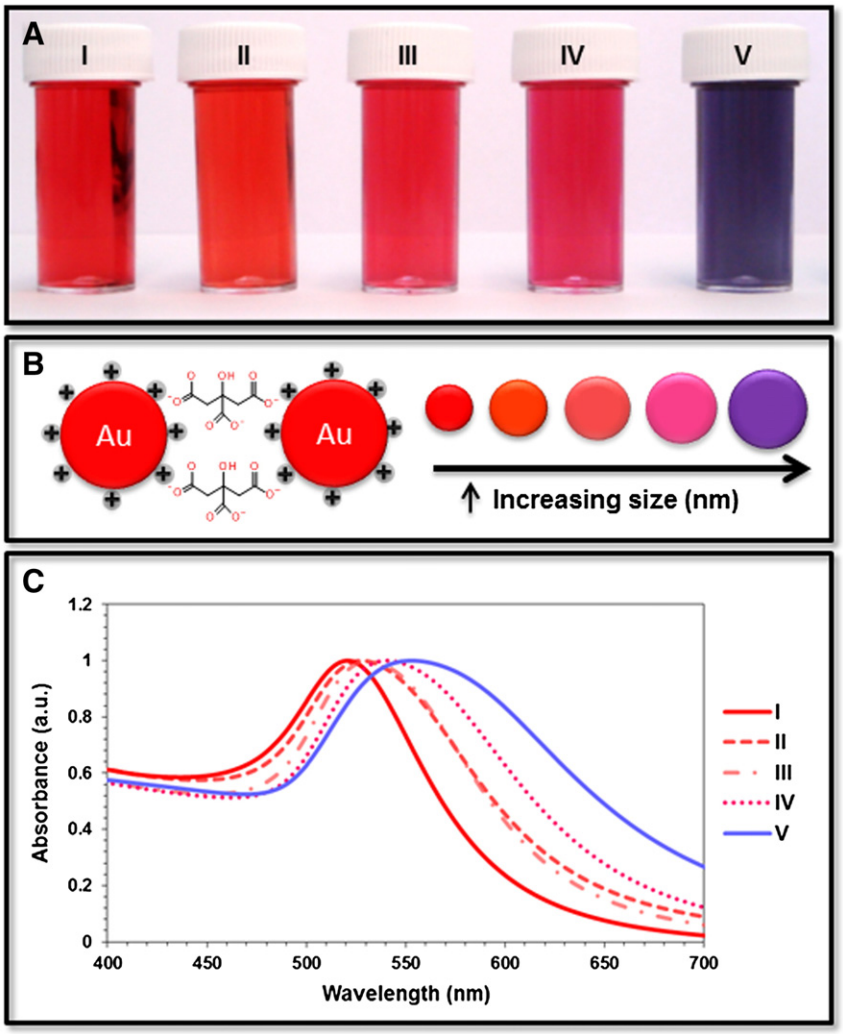

Figure 1. **(A-C).** Image of colloidal Au samples (colloidal samples I-V) after reduction with sodium citrate. Stability is achieved through electrostatic stabilization **(B)** with citrate ions ($C_3H_5OCOO_3^{3-}$), and the colors indicate different sized AuNPs with unique LSPR **(C)** in the UV–vis spectra for each Au sol.

Optimisation of AuNP concentration

Equal concentrations of colloidal Au were achieved through calculation and treatment steps using reported methods.[44] Briefly, the average number of Au atoms (N) in each spherical NP was estimated using (Eq. (2)), where D is the average core diameter, ρ is the density (19.3 g/cm^3) and M is the atomic weight of Au (197 g/mol) assuming a uniform spherical shape and fcc crystal structure.

$$N = \frac{\pi}{6}\frac{\rho}{M}D^3 = 30.89602\ D^3 \tag{2}$$

The molar concentration (C) of each Au sol was calculated using (Eq. (3)) by dividing the total number of Au atoms (N_{total}) in $HAuCl_4$ in solution over the mean number of Au atoms per NP (N), where V is the volume of the reaction solution (L) and N_A is Avogadro's number.

$$C = \frac{N_{total}}{NVN_A} \tag{3}$$

It is assumed that the reduction of $Au^{+3}{}_{(aq)}$ to $Au^{0}{}_{(s)}$ in Eq. (1) was 100% efficient. Stock solutions of 20 nM AuNPs were prepared by serial dilution of sample I, and centrifugation of samples II to V.[45] Briefly, AuNPs were transferred in to a 2 ml low binding eppendorf tube (Corning Inc., USA), and centrifuged for 20 min. A 5415R micro-centrifuge (Eppendorf, Germany) was used for samples I-III (e.g. 7500, 6500, 3000 g) and Mistral 3000i centrifuge (MSE, UK) for samples IV-V, respectively (e.g. 1500 g, 1000 g). The supernatant was carefully removed and centrifuged again, and the supernatant was discarded, and recombined with the original sample. The combined sample was centrifuged again, the supernatant discarded, and the AuNP pellet was dispersed by vortex in the

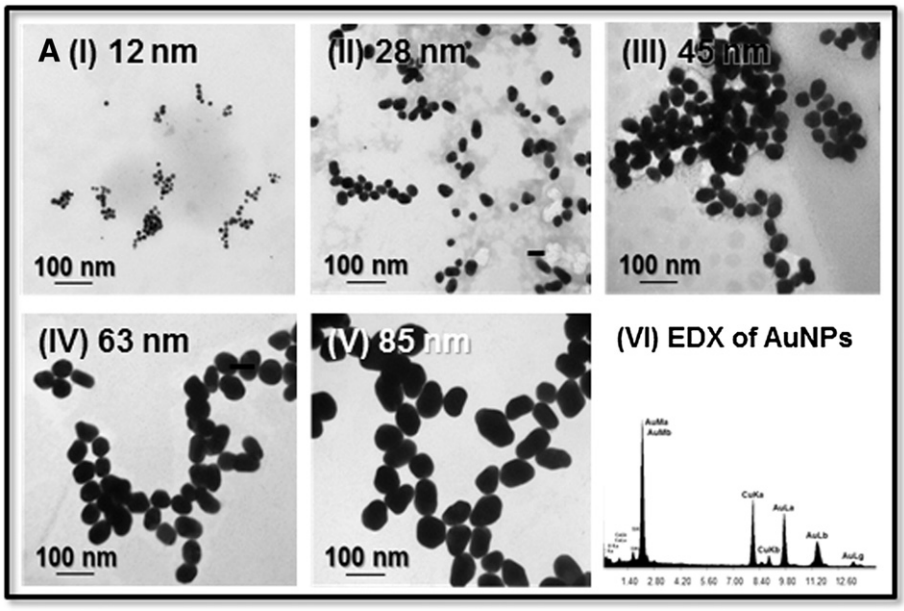

Figure 2. **(A).** TEM images of AuNPs (colloidal samples I-V) and EDX spectra (VI) show their elemental composition.

desired volume of dH_2O to produce a 20 nM stock. After a further centrifugation/resuspension step, the Au sol was measured by UV–vis and DLS to confirm that centrifugation had not aggregated the particles, and was similar to newly synthesized AuNPs.

Interactions of AuNPs in CWB

Blood collection and isolation of platelets and plasma

Ethical approval was granted (9215/001) in compliance with the Human Tissue Act, 2004. Whole blood was collected from healthy consenting volunteers using 2.7 ml blood collection tubes (BD Vacutainer) containing 0.109 M sodium citrate (3.8% w/v) as anti-coagulant. CWB was processed immediately after collection. To obtain platelet rich plasma (PRP), a 50 ml centrifuge tube containing 20 ml Lymphoprep™ (Axis-Shield, UK) and 20 ml CWB (1:1 ratio) was transferred in to a centrifuge tube without agitation or mixing (Figure 3, *A*). The tube was centrifuged at 200 g for 20 min at 20 °C. Platelets were collected from above the buffy layer and placed in to a sterile centrifuge tube followed by a hemocytometer count. The plasma fraction was collected and centrifuged again at 200 g for 20 min to obtain platelet poor plasma (PPP), which was carefully transferred in to sterile centrifuge tube prior to use.

Evaluation of AuNP interactions in PPP

A Zetasizer Nano-ZS (Malvern Ltd., UK) was used to measure dynamic light scattering (DLS) and zeta (ζ) potentials of AuNPs to determine their size and charge before and after incubation in PPP. 1 ml Au sol at 20 nM was incubated with 1 ml PPP in a sterile eppendorf tube for 1 h at 37 °C in 5% CO_2/95% humidified air. After 1 h the samples were centrifuged as described previously, and the supernatant discarded and 1 ml dH_2O was added to redisperse AuNPs by vortexing, and was repeated three times to remove excess PPP. Disposable capillary cells were used for DLS and ζ measurements, and were rinsed with dH_2O before introducing 500 μl AuNPs. The temperature was set to 25 °C, and allowed to equilibrate for 120 s. An average of three samples was used for DLS after 10-15 runs per cycle, and 20 runs per cycle to calculate ζ potentials using Smoluchowski's equation. An ELISA assay kit was used to quantify human fibrinogen (HFib) in the presence of AuNPs, and was used in accordance with the manufacturer's instructions (ICL Labs, USA, cat no. E-80FIB). Briefly, a standard calibration curve of HFib (400 ng/ml stock) was prepared in sample diluent, and 100 μl of standard was transferred in to a 96 well plate (n = 4). 166 μl AuNPs were added to 500 μl of PPP (0.66 nM) and incubated at 37 °C for 1 h. Each AuNP-PPP sample was centrifuged and resuspended in dH_2O and diluted 1:200 followed by incubation for 1 h in the microtitre plate. Each well was washed three times, and 100 μl anti-HFib-HRP was allowed to incubate for 30 min followed by further wash steps, and 100 μl TMB substrate solution was added and incubated in the dark for 10 min. 100 μl stop solution was added, and the optical density (OD) at 450 nm was measured using an Anthos 2010 (Biochrom Ltd., UK) plate reader.

Platelet aggregometry with AuNPs

Platelet aggregometry was performed using a platelet aggregation profiler, PAP-8E (Bio/Data Corporation, USA), and calibrated with PPP and PRP (200×10^6 platelets/ml) at 37 °C. Cuvettes with magnetic stirrers were prepared with 225 μl PRP and 25 μl AuNPs (2 nM), and 25 μl adenosine diphosphate (2 μM ADP) as a control. Each test was allowed to run for 10 min. Platelet morphology was also evaluated in the presence of AuNPs and after surface

modification (see 2.3.5) using scanning electron microscopy, and is presented in supplementary information (SI 1.1, Figure S1).

Thromboelastography (TEG®) and thrombin generation (TG)

A TEG® hemostasis analyzer measured viscoelastic changes of developing blood clots under low shear stress conditions to monitor blood coagulation and hemostasis (Figure 5, *A-D*). A TEG® 5000 analyzer (Haemonetics Corp, USA) was used to study CWB-AuNP interactions at 1.2 and 5 nM concentrations using disposable polystyrene TEG® cups and pins using defined parameters described in the supplementary section (SI 1.2 Table S1). Before each test, the analyzer was calibrated according to manufacturer's instructions. The cups were placed in the TEG® analyzer to equilibrate at 37 °C before experimentation. Colloidal AuNPs and 0.2 M $CaCl_2$ was incubated at 37 °C prior to testing. 20 and 85 μl of a 20 nM stock AuNP solution was added to TEG® cups followed by the addition of 320 and 255 μl of blood to obtain 1.2 and 5 nM concentrations. The solution was gently mixed in the TEG® cups followed by the addition of 20 μl $CaCl_2$ to initiate blood coagulation (final vol. 360 μl). All tests were measured immediately, and CWB in the absence of AuNPs was used as a control (n = 3 per condition). Further tests with AuNP (sample I = 12 nm particles) stock solutions were performed to monitor the influence of residual ions during their preparation and after resuspension in dH_2O. 20 μl supernatant and 0.25 nM $HAuCl_4$ was added to TEG® cups followed by CWB and $CaCl_2$ to understand the influence on blood coagulation (SI 1.3, Figure S2).

Surface modification of AuNPs

20 nM AuNPs (sample I) stock solutions was used to modify NPs with polyethylene glycol methyl ether thiol (PEG-thiol, Mw 2000) and 3-mercaptopropionic acid (3-MPA) as described in reported methods.[46] PEG-thiol (5 mM, 100 μl) and 3-MPA (5 mM, 900 μl) were prepared in sterile 1 ml dH_2O to generate mixed ligands. The solution was stirred for 30s and allowed to react overnight (18 h) at 4 °C. Each sample were centrifuged at 4000 g for 30 min to remove excess PEG-thiol and re-suspended in 1 ml dH_2O prior to experimentation. Bi-ligand modification was selected due to their stability in a range of pH and salt solutions, and free carboxylic groups for conjugation studies and future work. 10 μl HFib (10 mg/ml) was reacted with 990 μl AuNPs to yield a 10 μg/ml AuNP-HFib dispersion. Clopidogrel is a known anti-platelet agent and inhibitor of adenosine diphosphate (ADP) chemoreceptors on the platelet surface to prevent blood from clotting. 10 μl clopidogrel (5 mg/ml) was added to 990 μl AuNPs to yield a 5 μg/ml AuNP-clopidogrel dispersion, and is effective in the microgram concentration range. Fibronectin (Fn) is a glycoprotein present in the blood (~0.4 mg/ml), and is composed of multiple L-arginine-glycine-L-aspartic acid (RGD) tripeptide domains, which bind to integrin receptors on the cell membrane to direct cell fate, e.g. adhesion, migration and differentiation.[47] 10 μl RGD (1 mg/ml) was added to 990 μl AuNPs to yield a 1 μg/ml AuNP-RGD dispersion. Each AuNP dispersion was sonicated for 30 s, and incubated for 1 h (except PEG-thiol ~24 h) followed by centrifugation to remove any unbound material, and re-dispersed in 1 ml dH_2O. UV–vis measured peak LSPR, which indicated that the modification had been achieved prior to testing, and was used for TEG® as described previously. Surface modified AuNPs (1.2 nM) were compared with stock solutions of free ligands comprised of PEG-thiol, HFib, clopodigrel and RGD tripeptides. 20 μl of each solution was added to TEG® cups followed by the addition of 320 μl of CWB and 20 μl $CaCl_2$ and compared with AuNPs to understand their influence in the blood and role as a surface coating on the NP carrier (SI 1.4, Figure S3).

Table 1
AuNP size was compared with published data[43] vs. TEM measurements, and calculations were performed to standardize their molar concentration, *C*.

Sample	Reported size - TEM (nm)	Mean diameter - TEM (nm)	*N*	*C (mol/L)*
I	16.0	12.32 (±1.8)	5.78×10^4	86.5×10^{-9}
II	24.5	28.64 (±5.5)	7.26×10^5	6.89×10^{-9}
III	41.0	45.31 (±7.0)	2.87×10^6	1.74×10^{-9}
IV	71.5	63.25 (±8.6)	7.82×10^6	0.64×10^{-9}
V	97.5	85.96 (±10.9)	1.96×10^7	0.26×10^{-9}

Statistical analysis

Statistical analysis was performed using mean values, standard deviations for colloidal AuNPs (I-V) for particle characterization, plasma incubation, platelet aggregometry and TEG® analysis. One-way ANOVA tests were carried out in conjunction with Tukey and Duncan Post-Hoc tests using IBM SPSS Statistics v.24 software (Statistical Analysis System, Chicago, Illinois, USA). *indicates *P* values of <0.05 were considered to be significant when colloidal AuNPs were compared with controls.

Results

Characterization of AuNPs

Synthesis of colloidal Au produced stable sols identified by their unique color arising from different sized NPs (Figure 1, *A-C*). UV–vis spectra revealed strong signatures indicative of LSPR at 521 nm (I), 528 nm (II), 531 nm (III), 541 nm (IV) and 553 nm (V), which indicate the adsorption of light in the blue-green region of the spectrum. TEM analysis revealed the shape and size of AuNPs. Generally, spherical AuNPs became more irregular, and oval shaped with increasing size. High resolution images show spherical AuNPs in sample I with a uniform size of 12 nm, and sample II with a bimodal distribution and size of 28 nm (Figure 2, *A*). Sample III was mostly spherical with few irregularly shaped NPs, which had a uniform distribution of 45 nm, and sample IV contained oval and rod shaped NPs with a size of 63 nm. Sample V had fewer spherical NPs, and a uniform distribution at 85 nm in diameter. All samples, matched their predicted size and within the limit of error. EDX spectra confirmed that NP composition was derived from Au (Figure 2, *AVI*). Table 1 provides a summary of TEM data used to calculate the number of atoms (*N*) and molar concentration (*C*) to standardize each Au sol.

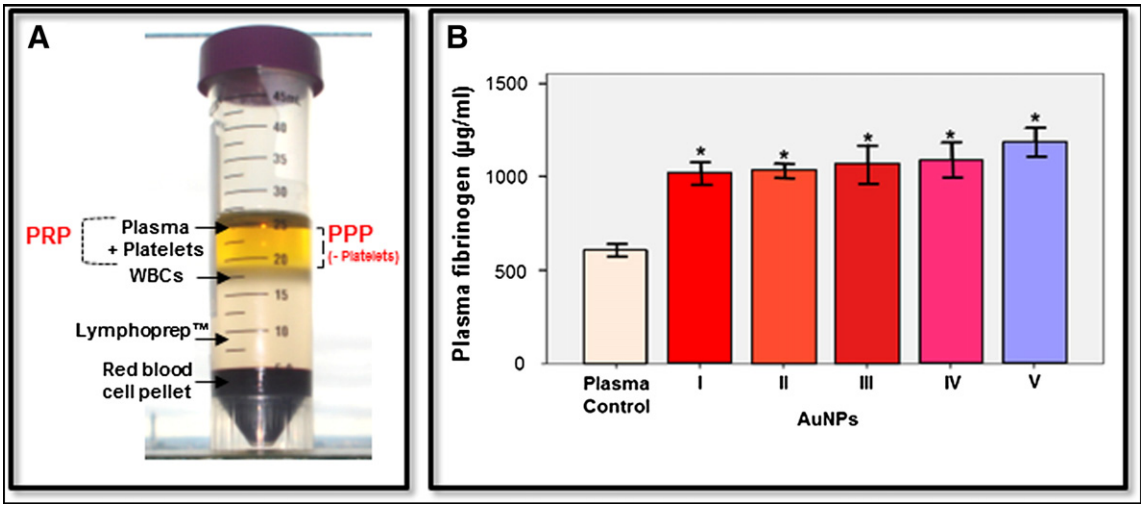

Figure 3. **(A-B).** Image **(A)** presents the isolation of PRP and PPP after centrifugation of CWB. HFib [µg/ml] with AuNPs (colloidal samples I-V) was determined through ELISA **(B)**, DLS and ELS.

Table 2
Highlights AuNP size and ζ potential after incubation for 1 h in PPP.

Sample	Hydrodynamic diameter (nm)		ζ potential (mV)	
	Before	After 1 h incubation*	Before	After 1 h incubation*
I	34.3 (±0.3)	162.4 (±6.7)	−39.8 (±0.4)	−19.1 (±0.9)
II	43.6 (±0.1)	110.4 (±4.0)	−40.6 (±1.1)	−25.3 (±0.3)
III	54.5 (±0.7)	139.6 (±7.7)	−38.4 (±0.9)	−29.0 (±0.1)
IV	73.8 (±3.9)	137.4 (±3.4)	−41.2 (±2.0)	−20.5 (±0.7)
V	104.6 (±0.7)	186.6 (±2.0)	−34.0 (±0.3)	−21.8 (±1.1)

* = $P < 0.0001$ when compared with AuNPs before incubation.

AuNP interactions in PPP

We studied AuNP interactions after isolation of PRP and PPP from CWB (Figure 3, *A*). AuNPs (I-V) were incubated in PPP for 1 h followed by ELISA to determine the level of HFib (Figure 3, *B*). Generally, the level of HFib bound to AuNPs almost doubled from 600 to 1000 µg/ml showing elevated levels when compared with plasma controls. However, the slight increase in HFib adsorption with AuNP size from 1000 to 1250 µg/ml was not significant. DLS measurements show that the AuNPs changed significantly with an increase in hydrodynamic size after incubation in PPP, doubling in size (Table 2) or more, and their mean intensity and size distributions are presented in the supplementary information (SI 1.5, Figure S4). ζ potentials calculate the electrophorectic mobility of AuNPs as a streaming potential surrounding the electric double layer by oscillating electric fields. Mean ζ potentials changed significantly before (−39 ± 3 mV) and after incubation (−23 ± 4 mV) with an increase in NP size, and decrease in negative charge. Sample I showed the largest change in diameter with almost a 5-fold increase from 34 to 162 nm, and a 50% reduction in ζ potential from −39 to −19 mV. Samples II-IV all doubled in size or more whilst ζ potentials show a similar decrease in negativity. Sample V showed the smallest increase in diameter and decrease in negativity.

AuNP interactions in PRP

The principle of platelet aggregometry is to measure the extent of aggregation using agonists (platelet activators), e.g. ADP. Aggregation is recorded as a function of % light transmission through changes in OD (Figure 4, *A*). In Figure 4, *B*, ADP initiated a rapid response causing platelets to aggregate after 1 min with 60% aggregation at 2 min, and 70% after 10 min (Figure 4, *B*). The level of platelet aggregation (%) in the presence of AuNPs was low in each of the samples tested as follows: (I) 12%, (II) 13%, (III) 9%, (IV) 14%, (V) 11% after 10 min with some aggregation due to shear forces generated by the magnetic beads. We compared aggregometry data with platelet morphology using SEM in the presence of AuNPs and after modification with PEG-thiol, and RGD along with a strong agonist control, collagen type I (SI 1.1, Figure S1). This work suggests that platelet activation and aggregation occurs via surface bound ligands, and could link platelet aggregometry to TEG® data and warrants future study.

TEG® to monitor blood-AuNP interactions

TEG® provided information on blood coagulation kinetics using a small amount of blood placed inside a cup to monitor clot formation (Figure 5, *A-D*). We studied coagulation in the presence of AuNPs obtained in all of the colloidal samples (I-V) at concentrations of 1.2 and 5 nM, which had the same size and charge characteristics as described earlier to measure their influence on clot initiation (R), clot build up and kinetics (α-angle°) and overall clot strength (MA). Analysis of blood with 1.2 nM AuNPs shows no statistical significance in any of the parameters tested (Figure 6, *A-C*). Studies with 5 nM AuNPs show a significant decrease in R time in samples III and V (7.8 ± 0.3 min) when compared with blood without NPs (12.5 ± 1 min) indicating a faster rate of clot formation and prothrombotic state (Figure 6, *D-F*). No difference in α-angle was apparent. There was a significant reduction in MA in samples II (44 ± 2 mm), III (48 ± 1.3 mm) and IV (49 ±

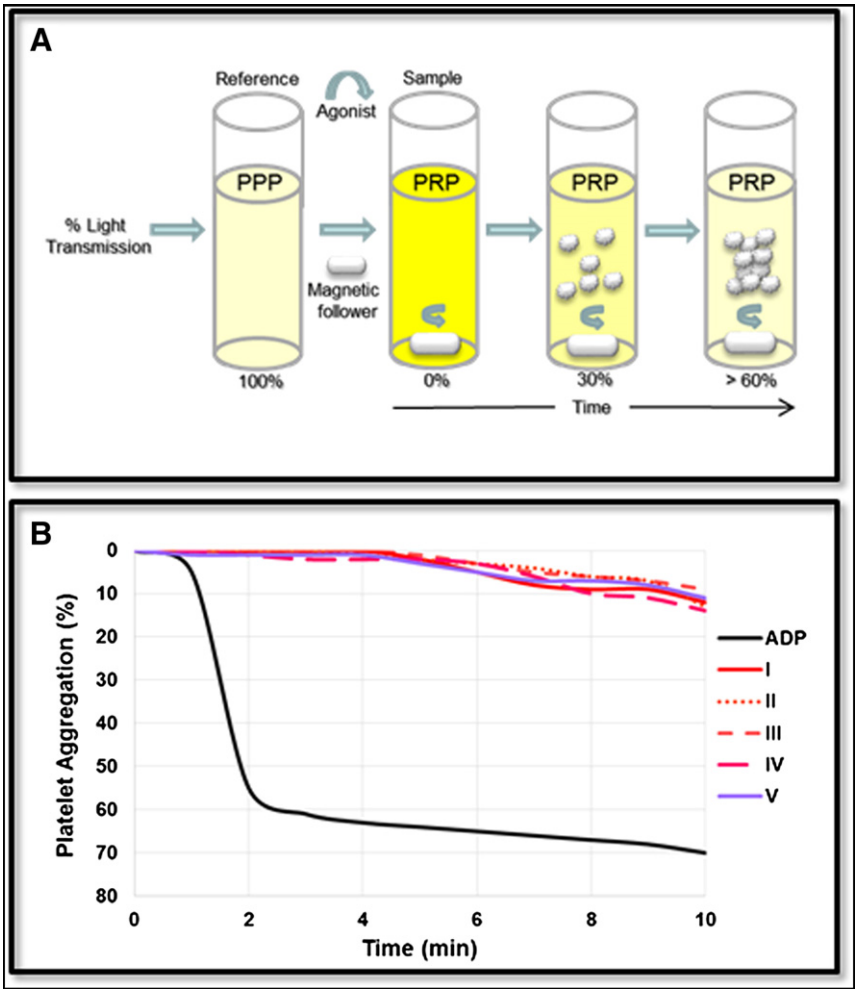

Figure 4. (**A** and **B**). Platelet aggregometry tests with AuNPs (colloidal samples I-V) over 10 min.

0.4 mm) compared to controls (58.5 ± 0.4 mm). There was no clear trend in relation to AuNP size, but a concentration dependent effect from 1.2 to 5 nM. TEG® parameters also provided data on thrombus generation (TG), maximum rate (MRTG), and time to reach the maximum rate of TG (TMRTG), which correlates with thrombin-anti-thrombin complex (TAT) used in thrombin generation assay, which is described in detail in the supplementary sections (SI 1.6, Table S2).[48]

Surface modification of AuNPs

We selected the lower concentration of 1.2 nM AuNPs to study the influence of surface modification using sample I (AuNP I) comprised of 12 nm particles to investigate their interactions with surface bound ligands in CWB (Figure 7, *A-G*). Each ligand was selected on the basis of bioactivity as follows; 1) to prevent protein adsorption (PEG-thiol), 2) pre-condition the corona (HFib), 3) immobilize platelet inhibitors (clopidogrel), and 4) immobilize activators of platelet function (RGD). Analysis of CWB and untreated (bare) AuNPs before and after modification with PEG, HFIB, and Clop show no difference in R time values. However, blood containing AuNP-RGD presents a significant decrease in R time (8.25 ± 0.25 min) when compared with untreated AuNPs (12 ± 0.7 min) indicating a faster, prothrombotic response. A reduction in clot build up and kinetics was apparent with AuNP-PEG (26 ± 0.5°), AuNP-HFib (24 ± 0.75°), and AuNP-Clop (22 ± 1°) when compared with untreated AuNPs (33 ± 1°). The same trends were apparent in overall MA compared with AuNP-PEG (53 ± 0.4 mm), AuNP-HFib (44 ± 0.6 mm), and AuNP-Clop (45 ± 1.6 mm) when compared with untreated AuNPs (59 ±0.6 mm). Their influence on MRTG, TMRTG and TG, are described in detail in the supplementary sections (SI 1.6, Table S3).

Discussion

We synthesized a range of AuNPs with varying size to study their interactions in CWB. UV/vis spectroscopy and TEM was used to analyze their LSPR, core diameter, shape and composition, which confirmed that smaller NPs (I-III) were spherical and became more irregular with increasing size (IV-V).[43] A two-step seed mediated approach can be used to increase their size range and warrants future study. AuNPs doubled (or more) in size when incubated in plasma and DLS differed from TEM as size can be overestimated depending on shape distribution and Brownian motion. Moreover, smaller NPs

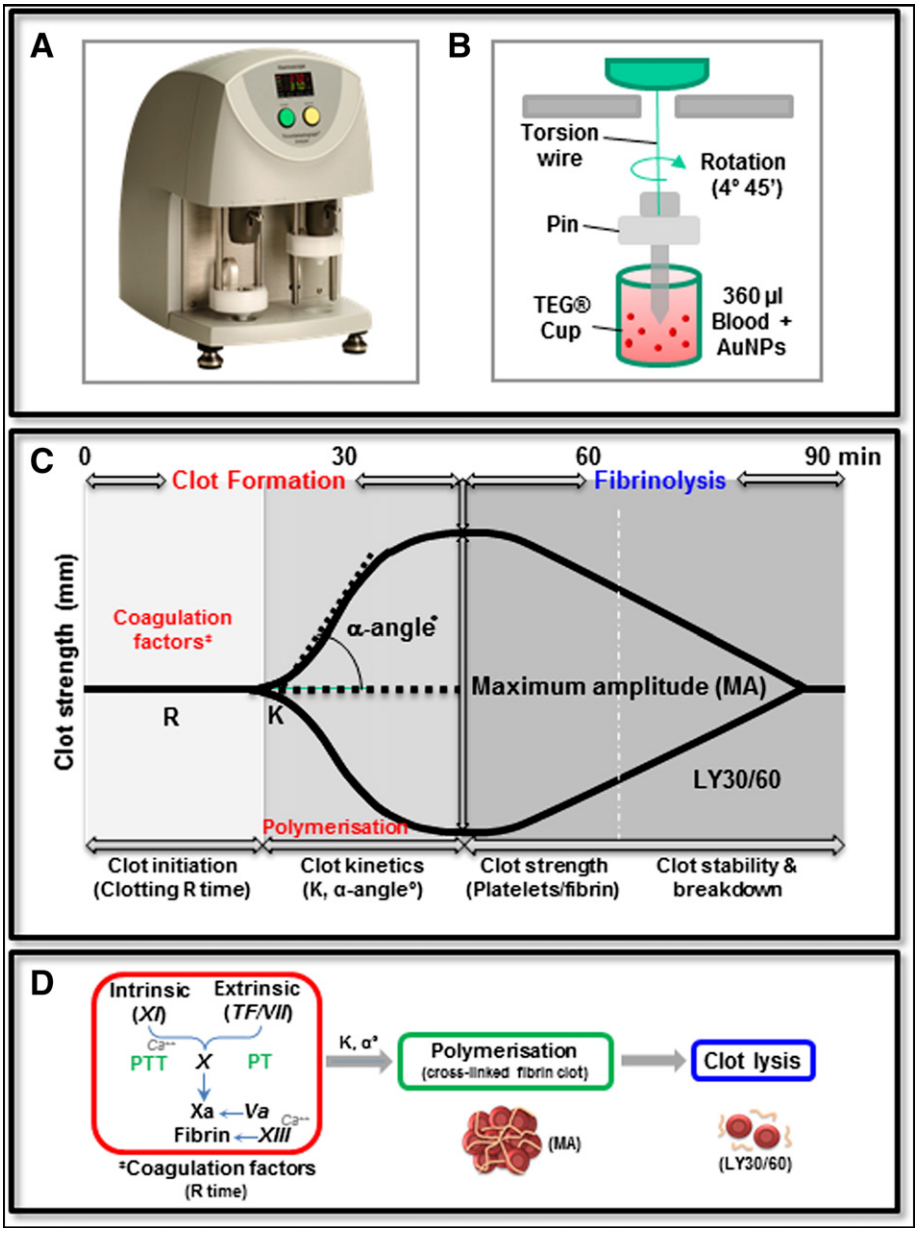

Figure 5. **(A-D).** A TEG® hemostasis analyzer **(A)** was used to measure AuNP interactions in blood placed inside a TEG® cup, which oscillates at a set speed and angle of 4°45′ **(B)**. A pin is immersed in the cup causing oscillations proportional to clot strength. The TEG® trace **(C)** measures clot initiation and influence of coagulation factors (R), clot formation (K, α-angle°), and clot strength (MA) and lysis (LY30). Clot initiation (R) activates the intrinsic (XI + Ca^{2+}) and extrinsic (tissue factor/VII) pathway through conversion of factors X in to Xa (D). For comparison, aPTT and PT assays measure both pathways in isolation. This leads to the common pathway via thrombin and formation of fibrin. Factor XIII initiates cross-linking of fibrin to activate platelet adhesion to form a stable clot.

experience greater changes in hydrodynamic diameter with the formation of protein corona.[10,49] ζ measurements of untreated AuNPs show negative potentials due to charge stabilization with citrate ions ($C_3H_5OCOO_3^{3-}$). After incubation, a reduction in ζ was apparent due to the effects of protein adsorption and screening of the charge. Previous studies report that HFib is abundant in the corona of AuNPs, and binds through electrostatics or thiol (−SH) groups via cysteine resulting in Au-S bond formation.[50–51] We quantified the level of HFib with AuNPs, and found that the concentration almost doubled indicating a very strong level of interaction. Platelet aggregation tests show little change in the presence of AuNPs after 10 min similar to reported data.[16,19] Recently, AuNPs have been shown to have proaggregatory effects after activation of platelets with ADP, and show size dependent reactions with 20 nm particles having the greatest influence on platelet factor 4 release.[52] Activated platelets bind to fibrinogen via $\alpha_{IIb}\beta_3$ integrin receptors and cleavage by thrombin in to α or β chain fibrinopeptides self-assemble in to a fibrin network resulting in a platelet plug.[53–54] Moreover, since AuNPs show little interaction with inactivate platelets, the level of pre-activation by NPs is an important parameter that warrants further study.

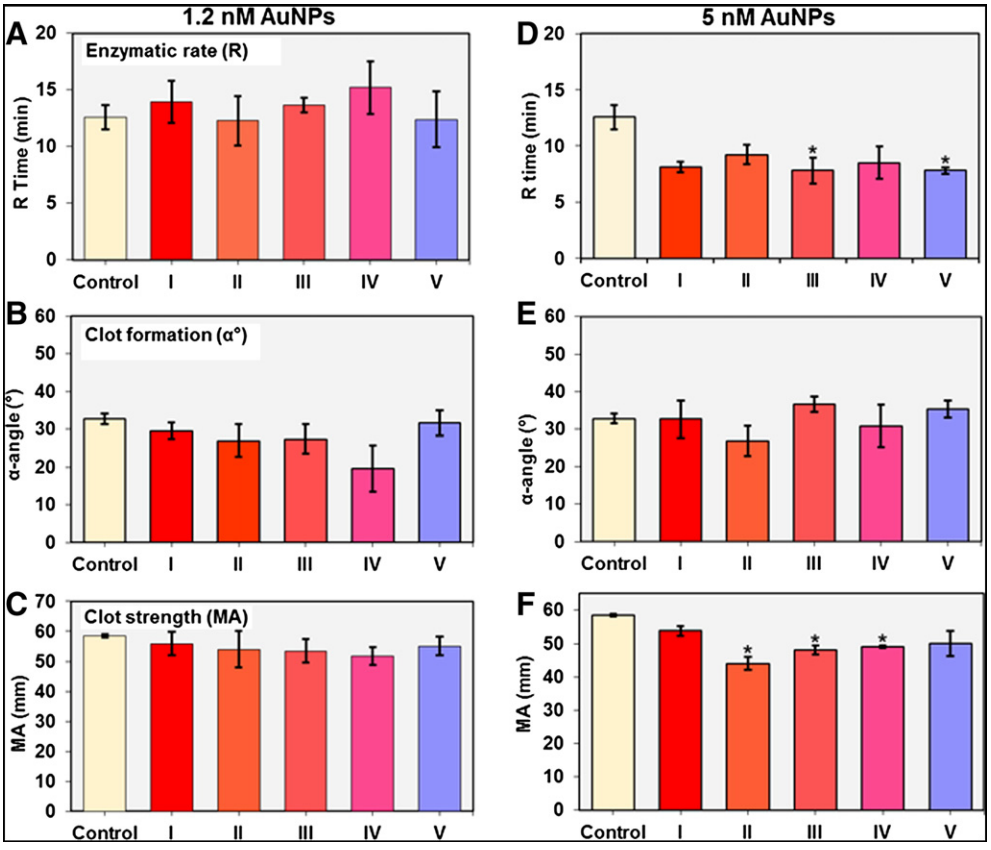

Figure 6. **(A-F).** TEG® measurement parameters **(A, D)** R time, **(B, E)** α-angle° and **(C, F)** MA in CWB (control) vs. AuNPs (colloidal samples I-V) at 1.2 and 5 nM concentrations. * = $P < 0.05$.

TEG® was used to study the influence of AuNPs in the blood and sodium citrate is a known anticoagulant, which chelates calcium ions (Ca^{2+}) to disrupt clotting by inactivating co-factors and platelets.[41] Restoration of hemostasis is achieved by adding $CaCl_2$ (Ca^{2+}) to activate blood coagulation. TEG® studies with 1.2 nM AuNPs had little influence on blood coagulation kinetics. However, large differences were apparent at higher concentrations with a faster R time values from 12 to 15 min to 8-9 min for 1.2 nM and 5 nM, respectively. R time is a physical representation of standard clotting studies, and the time taken for the clot to span from the cup edge to the pin. Both samples III (45 nm) and V (85 nm) had the greatest influence on R time (7.8 min), and α-angle (36.5°) resulting in a prothrombotic response, and faster rate of clot formation measured by the speed of fibrin build-up and extent of cross-linking. It is known that HFib undergoes self-assembly on flat Au surfaces to form nanofibrils.[54] When bound to AuNPs, conformational changes could disrupt the trinodular structure of HFib (9 × 47.5 × 6 nm), which has similar dimensions to NPs. This could attract coagulation factors to the surface by exposing binding sites or epitopes to enhance enzyme activity, and warrants further investigation. MA is a measure of fibrin and platelet bonding via $\alpha_{IIb}\beta_3$ receptors and represents the total strength of the fibrin clot, and correlates with platelet function. Generally, clot strength decreased significantly in the presence of AuNPs, and the greatest reduction was apparent in sample II (28 nm), III (45 nm) and IV (63 nm). Perhaps AuNPs bind greater amounts of HFib with a strong affinity due to the increased surface area causing aggregation of AuNPs, which could hinder thrombin activity, and reduce the level of fibrin available for cross-linking reactions to reduce platelet activity resulting in a weaker clot. Moreover, thrombus generation (TG) was significantly reduced, which may account for weaker clot formation. More studies are needed to examine the procoagulant effects of AuNPs on enzyme activity, fibrin assembly and clot stability, which will influence fibrinolysis impacting on cell uptake, clearance and accumulation in the tissues.[55–56]

We modified AuNPs to tailor their bioactivity as an example of targeted and site specific delivery to study the influence of non-specific protein adsorption (PEG-thiol), protein corona (HFib), and inhibition (clopidogrel) or activation (RGD) of platelet function. AuNP-PEG had no effect on R time, but reduced clot formation (α-angle°) and strength (MA). It is known that PEG increases their circulation lifetime in the blood when used in combination with nanocarriers or drugs. AuNP-PEG has been shown to slightly influence the amount of bound proteins, and some level of binding has been found to be essential to direct cell uptake as a prerequisite for specific targeting.[25,56] AuNP-HFib had little influence on R values, but severely disrupted clot formation (α-angle°) and strength (MA), similar to that seen previously, indicating that HFib bound to AuNPs plays a key role in the prevention of fibrin build-up, polymerization

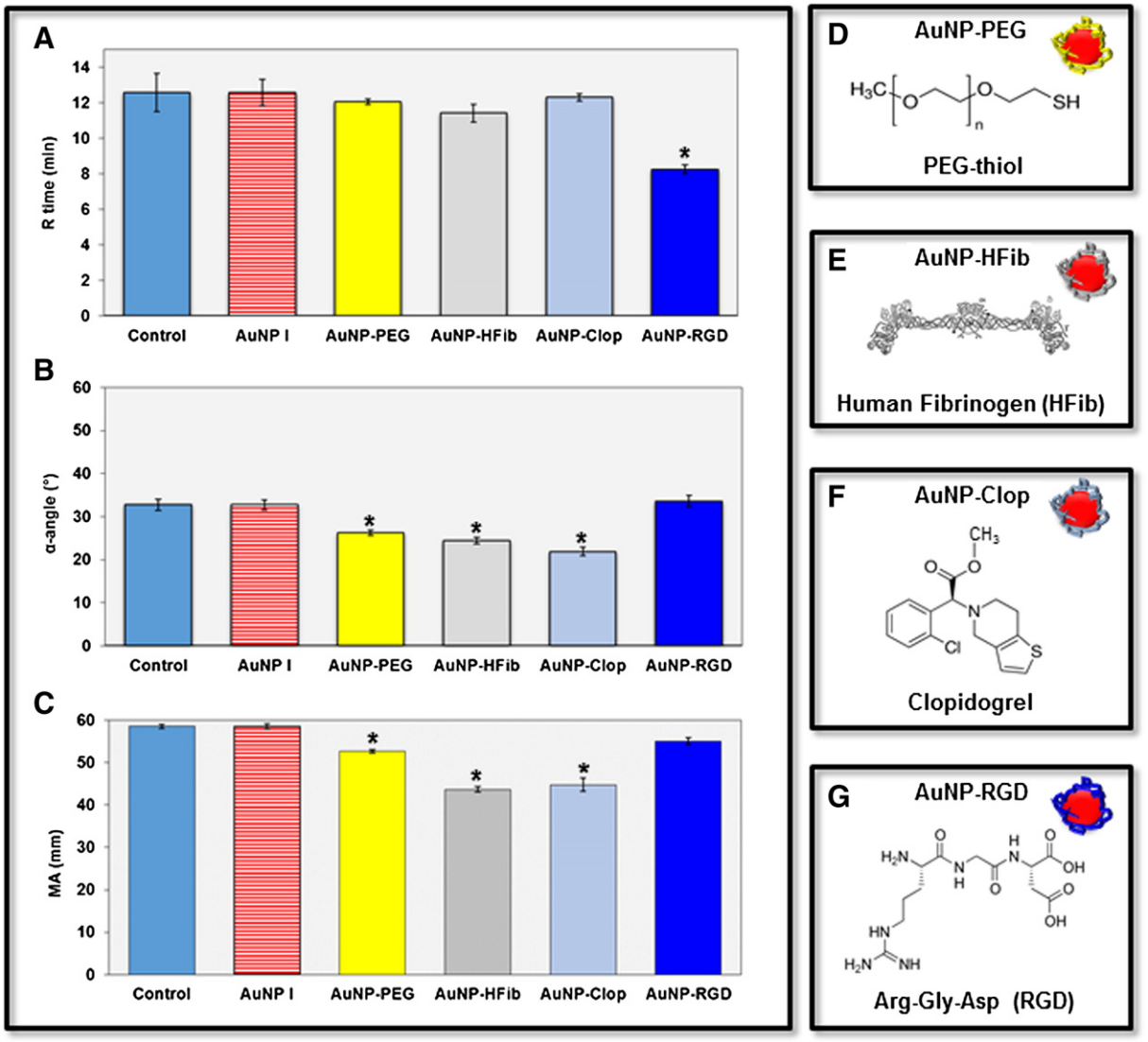

Figure 7. **(A-G).** TEG® measurement parameters **(A)** R time, **(B)** α-angle° and **(C)** MA in CWB (control) vs. untreated AuNPs (colloidal sample I only at 1.2 nM) and after modification with AuNP-PEG **(D)**, ≠AuNP-HFib **(E)**, AuNP-Clop **(F)** and AuNP-RGD **(G)**. ≠Image E is adapted from Ref.[55] * = $P < 0.05$.

and cross-linking and adhesion of platelets to fibrin. Similarly, AuNP-Clop impaired blood clot formation and strength as clopidogrel is a known antiplatelet agent and prodrug, which inhibits ADP receptors on platelets, and is used to inhibit blood clotting and prevent stent-mediated thrombosis.[57] AuNP-RGD was found to have prothrombotic effects, which have significantly faster R times with no effect on clot formation and strength. RGD is active ligand for adhesive matrix proteins such as HFib and Fn, which bind to $\alpha_{IIb}\beta_3$ receptors on activated platelets, which are essential for aggregation.[58]

Our results demonstrate that TEG® is well suited to study AuNP interactions in CWB, and gives dynamic information on blood coagulation in vitro. When used as a rapid screening tool TEG® offers a detailed analysis of thrombogenicity presenting an ideal platform to select test candidates (e.g. charge and bioactivity) and optimal formulations to screen their safety and efficacy in human blood, and can potentially replace the need for non-essential animal tests. TEG® is already used in the clinic to determine anticoagulant and procoagulant states and deficiencies in fibrinogen and platelet function. Such tests can fill the knowledge gaps between in vitro test methodology and in vivo performance to produce data, which is predictive of the clinical situation.[36] Much effort is needed to standardize TEG® with other sensitive methods to understand how NPs effect the level of activation of co-factors and platelets, which would represent a significant breakthrough in understanding hematological events at the nano-bio interface. For example, specific targeting of the coagulation pathways, e.g. factors XI or VII could lead to new therapies for coagulation disorders, e.g. treatment of cardiovascular disease, hemophilia or blood cancers using nano-drugs or screening new tools for nano-surgery and develop haemostatic agents or improve diagnostic tests with enhanced sensitivity.

In summary, we characterized AuNPs to study their interactions in plasma and in human CWB using TEG® and demonstrate prothrombogenic effects, and reduction in R values (time until initial clot formation) in a concentration dependent

manner. Size effects exhibit a non-linear trend with 45 and 85 nm sized particles resulting in a faster prothrombotic response. Clot strength decreased significantly with NP size the greatest reduction being with 28 nm particles. We investigated tailored surface modification of AuNPs in the blood further to focus on their biological activity. AuNP-RGD possessed procoagulant activity, while PEG-thiol, HFib and clopidogrel influenced clot formation, fibrin build-up and platelet activity. Such tests can be used to fill the knowledge gaps in thrombogenicity, and fully optimize new nanoformulations in vitro to predict in vivo haemocompatibility.

Appendix A. Supplementary data

Supplementary data to this article can be found online at http://dx.doi.org/10.1016/j.nano.2017.01.019.

References

1. Dreaden EC, Alkilany AM, Huang X, Murphy CJ, El-Sayed MA. The golden age: gold nanoparticles for biomedicine. *Chem Soc Rev* 2012;**41**:2740.
2. Giljohann DA, Seferos DS, Daniel WL, Massich MD, Patel PC, Mirkin CA. Gold nanoparticles for biology and medicine. *Angew Chem Int Ed Eng* 2010;**49**:3280-94.
3. Arvizo R, Bhattacharya R, Mukherjee P. Gold nanoparticles: opportunities and challenges in nanomedicine. *Expert Opin Drug Deliv* 2010;**7**:753-63.
4. Jain S, Hirst DG, O'Sullivan JM. Gold nanoparticles as novel agents for cancer therapy. *Radiol* 2012;**85**:101-13.
5. Aggarwal P, Hall JB, McLeland CB, Dobrovolskaia MA, McNeil SE. Nanoparticle interaction with plasma proteins as it relates to particle biodistribution, biocompatibility and therapeutic efficacy. *Adv Drug Deliv Rev* 2009;**61**:428-37.
6. Soenen SJ, Rivera-Gil P, Montenegro JM, Parak WJ, De Smedt SC, Braeckmans K. Cellular toxicity of inorganic nanoparticles: common aspects and guidelines for improved nanotoxicity evaluation. *Nano Today* 2011;**6**:446-65.
7. Sutherland DS, Broberg M, Nygren H, Kasemo B. Influence of nanoscale surface topography and chemistry on the functional behaviour of an adsorbed model macromolecule. *Macromol Biosci* 2001;**1**:270-3.
8. Vroman L. Effect of adsorbed proteins on the wettability of hydrophilic and hydrophobic solids. *Nature* 1962;**196**:476-7.
9. Brewer SH, Glomm WR, Johnson MC, Knag MK, Franzen S. Probing BSA binding to citrate-coated gold nanoparticles and surfaces. *Langmuir* 2005;**21**:9303-7.
10. Lacerda SH, Park JJ, Meuse C, Pristinski D, Becker ML, Karim A, et al. Interaction of gold nanoparticles with common human blood proteins. *ACS Nano* 2010;**4**:365-79.
11. Dobrovolskaia MA, McNeil SE. Immunological properties of engineered nanomaterials. *Nat Nanotechnol* 2007;**2**:469-78.
12. Fadeel B, Garcia-Bennett AE. Better safe than sorry: understanding the toxicological properties of inorganic nanoparticles manufactured for biomedical applications. *Adv Drug Deliv Rev* 2010;**62**:362-74.
13. Hussain S, Vanoirbeek JA, Hoet PH. Interactions of nanomaterials with the immune system. *Wiley Interdiscip Rev Nanomed Nanobiotechnol* 2012;**4**:169-83.
14. Mayer A, Vadon M, Rinner B, Novak A, Wintersteiger R, Fröhlich E. The role of nanoparticle size in haemocompatibility. *Toxicology* 2009;**258**:2-3 [139-47].
15. Ilinskaya AN, Dobrovolskaia MA. Nanoparticles and the blood coagulation system. Part II: safety concerns. *Nanomedicine (London)* 2013;**6**:969-81.
16. Fröhlich E. Action of nanoparticles on platelet activation and plasmatic coagulation. *Curr Med Chem* 2016;**23**:408-30.
17. Sperling RA, Parak WJ. Surface modification, functionalization and bioconjugation of colloidal inorganic nanoparticles. *Math Phys Eng Sci* 2010;**368**:1333-83.
18. Lazarovits J, Chen YY, Sykes EA, Chan WCW. Nanoparticle-blood interactions: the implications on solid tumour targeting. *Chem Commun* 2015;**51**:2756-67.
19. Dobrovolskaia MA, Patri AK, Zheng J, Clogston JD, Ayub N, Aggarwal P, et al. Interaction of colloidal gold nanoparticles with human blood: effects on particle size and analysis of plasma protein binding profiles. *Nanomedicine* 2009;**5**:106-17.
20. Casals E, Pfaller T, Duschl A, Oostingh GJ, Puntes V. Time evolution of the nanoparticle protein corona. *ACS Nano* 2010;**4**:3623-32.
21. Benetti F, Fedel M, Minati L, Speranza G, Migliaresi C. Gold nanoparticles: role of size and surface chemistry on blood protein adsorption. *J Nanopart Res* 2013;**15**:1694-703.
22. Goy-López S, Juárez J, Alatorre-Meda M, Casals E, Puntes VF, Taboada P, et al. Physicochemical characteristics of protein-NP bioconjugates: the role of particle curvature and solution conditions on human serum albumin conformation and fibrillogenesis inhibition. *Langmuir* 2012;**28**:9113-26.
23. Walkey CD, Olsen JB, Song F, Liu R, Guo H, Olsen DW, et al. Protein corona fingerprinting predicts the cellular interaction of gold and silver nanoparticles. *ACS Nano* 2014;**8**:2439-55.
24. Khan S, Gupta A, Verma NC, Nandi CK. Kinetics of protein adsorption on gold nanoparticle with variable protein structure and nanoparticle size. *J Chem Phys* 2015;**143**:164709.
25. Dobrovolskaia MA, Neun BW, Man S, Ye X, Hansen M, Patri AK, et al. Protein corona composition does not accurately predict haemocompatibility of colloidal gold nanoparticles. *Nanomedicine* 2014;**10**:1453-63.
26. Szymusiak M, Donovan AJ, Smith SA, Ransom R, Shen H, Kalkowski J, et al. Colloidal confinement of polyphosphate on gold nanoparticles robustly activates the contact pathway of blood coagulation. *Bioconjug Chem* 2016;**27**:102-9.
27. Tian Y, Zhao Y, Zheng W, Zhang W, Jiang X. Antithrombotic functions of small molecule-capped gold nanoparticles. *Nanoscale* 2014;**6**:8543-50.
28. Ehmann HMA, Breitwieser D, Winter S, Gspan C, Koraimann G, Maver U, et al. Gold nanoparticles in the engineering of antibacterial and anticoagulant surfaces. *Carbohydr Polym* 2015;**117**:34-42.
29. Sanfins E, Augustsson C, Dahlbäck B, Linse S, Cedervall T. Size-dependent effects of nanoparticles on enzymes in the blood coagulation cascade. *Nano Lett* 2014;**14**:4736-44.
30. Park MS, Martini WZ, Dubick MA, Salinas J, Butenas S, Kheirabadi BS, et al. Thromboelastography as a better indicator of Postinjury Hypercoagulable state than prothrombin time or activated partial thromboplastin time. *J Trauma* 2009;**67**:266-76.
31. Gorbet MB, Sefton MV. Biomaterial-associated thrombosis: roles of coagulation factors, complement, platelets and leukocytes. *Biomaterials* 2004;**25**:5681703.
32. Vogler EA, Siedlecki CA. Contact activation of blood-plasma coagulation. *Biomaterials* 2009;**30**:1857-69.
33. Narani K. TEG® in the perioperative period. *Anaesth* 2005;**49**:89-95.
34. Peng HT. Thromboelastographic study of biomaterials. *Appl Biomater* 2010;**94**:469-85.
35. Trapani L. Thromboelastography: current applications, future directions. *Anaest* 2013;**3**:23.
36. Shankarraman V, Davis-Gorman G, Copeland JG, Caplan MR, McDonagh PF. Standardized methods to quantify thrombogenicity of blood-contacting materials via thromboelastography. *Appl Biomater* 2012;**100**:230-8.

37. de Mel A, Naghavi N, Cousins BG, Clatworthy I, Hamilton G, Darbyshire A, et al. Nitric oxide-eluting nanocomposite for cardiovascular implants. *J Mater Sci Mater Med* 2014;**25**:917-29.
38. Steuer H, Krastev R, Lembert N. Metallic oxide nanoparticles stimulate blood coagulation independent of their surface charge. *Appl Biomater* 2014;**102**:897-902.
39. Libutti SK, Paciotti GF, Byrnes AA, Alexander Jr HR, Gannon WE, Walker M, et al. Phase I and pharmacokinetic studies of CYT-6091, a novel PEGylated colloidal gold-rhTNF nanomedicine. *Clin Cancer Res* 2010;**16**:6139-49.
40. Pilot study of AuroLase therapy in refractory and/or recurrent tumors of the head and neck. http://clinicaltrials.gov/ct2/show/NCT00848042 [accessed Jul 2016].
41. Mann KG, Whelihan MF, Butenas S, Orfeo T. Citrate anticoagulation and the dynamics of thrombin generation. *J Thromb Haemost* 2007;**5**:2055-61.
42. Turkevich J, Stevenson PC, Hillier J. A study of the nucleation and growth processes in the synthesis of colloidal gold. *Discuss Faraday Soc* 1951;**55-75**.
43. Frens G. Controlled nucleation for the regulation of the particle size in monodisperse gold suspensions. *Nature* 1973;**241**:20-2.
44. Liu XO, Atwater M, Wang JH, Huo Q. Extinction coefficient of gold nanoparticles with different sizes and different capping ligands. *Biointerfaces* 2007;**58**:3-7.
45. Balasubramanian SK, Yang L, Yung LY, Ong CN, Ong WY, Yu LE. Characterization, purification, and stability of gold nanoparticles. *Biomaterials* 2010;**34**:9023-30.
46. Gao J, Huang X, Liu H, Zan F, Ren J. Colloidal stability of gold nanoparticles modified with thiol compounds: bioconjugation and application in cancer cell imaging. *Langmuir* 2012;**28**:4464-71.
47. Jenney CR, Anderson JM. Adsorbed serum proteins responsible for surface dependent human macrophage behavior. *J Biomed Mater Res* 2000;**49**(4):435-47.
48. Rivard GE, Brummel-Ziedins KE, Mann KG, Fan L, Hofer A, Cohen E. Evaluation of the profile of thrombin generation during the process of whole blood clotting as assessed by thrombelastography. *J Thromb Haemost* 2005;**3**:2039-43.
49. Khlebtsov BN, Khlebtsov NG. On the measurement of gold nanoparticle sizes by the dynamic light scattering method. *Colloid J* 2011;**73**:118-27.
50. Schäffler M, Semmler-Behnke M, Sarioglu H, Takenaka S, Wenk A, Schleh C, et al. Serum protein identification and quantification of the corona of 5, 15 and 80 nm gold nanoparticles. *Nanotechnology* 2013;**24**:265103.
51. Deb S, Patra HK, Lahiri P, Dasgupta AK, Chakrabarti K, Chaudhuri U. Multistability in platelets and their response to gold nanoparticles. *Nanomedicine* 2011;**7**:376-84.
52. Chen G, Ni N, Zhou J, Chuang YJ, Wang B, Pan Z, et al. Fibrinogen clot induced by gold-nanoparticle in vitro. *J Nanosci Nanotechnol* 2011;**11**:74-81.
53. Lefkovits J, Plow EF, Topol EJ. Platelet glycoprotein IIb/IIIa receptors in cardiovascular medicine. *Med* 1995;**332**:1553-9.
54. Chen G, Ni N, Wang B, Xu B. Fibrinogen nanofibril growth and self-assembly on Au (1,1,1) surface in the absence of thrombin. *ChemPhysChem* 2010;**11**:565-8.
55. Côté HC, Lord ST, Pratt KP. γ-chain Dysfibrinogenemias: molecular structure–function relationships of naturally occurring mutations in the γ chain of human fibrinogen. *Blood* 1998;**92**:2195-212.
56. Minet V, Alpan L, Mullier F, Toussaint O, Lucas S, Dogné JM, et al. The euglobulin clot lysis time to assess the impact of nanoparticles on fibrinolysis. *J Nanopart Res* 2015;**17**:317.
57. Schöttler S, Becker G, Winzen S, Steinbach T, Mohr K, Landfester K, et al. Protein adsorption is required for stealth effect of poly(ethylene glycol)- and poly(phosphoester)-coated nanocarriers. *Nat Nanotechnol* 2016;**11**:372-7.
58. Ko T-M, Lin J-C, Cooper SL. Surface characterization and platelet adhesion studies of plasma-sulfonated polyethylene. *Biomaterials* 1993;**14**(9):657-64.